Interaction induced hybridization of Majorana zero modes in a coupled quantum-dot–superconducting-nanowire hybrid system

L. S. Ricco,[1,*] Y. Marques,[2] J. E. Sanches,[1] I. A. Shelykh,[2,3] and A. C. Seridonio[1,4,†]

[1]*Department of Physics and Chemistry, School of Engineering, São Paulo State University (Unesp), 15385-000 Ilha Solteira-SP, Brazil*

[2]*ITMO University, St. Petersburg 197101, Russia*

[3]*Science Institute, University of Iceland, Dunhagi-3, IS-107 Reykjavik, Iceland*

[4]*IGCE, Department of Physics, São Paulo State University (Unesp), 13506-970 Rio Claro-SP, Brazil*

(Received 13 June 2020; revised 19 September 2020; accepted 21 September 2020; published 5 October 2020)

We study the low-energy transport properties of a hybrid device composed by a native quantum dot coupled to both ends of a topological superconducting nanowire section hosting Majorana zero modes. The account of the coupling between the dot and the farthest Majorana zero mode allows one to introduce the topological quality factor, characterizing the level of topological protection in the system. We demonstrate that the Coulomb interaction between the dot and the topological superconducting section leads to the onset of the additional overlap of the wave functions describing the Majorana zero modes, leading to the formation of trivial Andreev bound states even for spatially well-separated Majoranas. This leads to the spoiling of the quality factor and introduces a constraint for the braiding process required to perform topological quantum computing operations.

DOI: 10.1103/PhysRevB.102.165104

I. INTRODUCTION

Errors coming from quantum decoherence are undoubtedly one of the most significant obstacles for successful realization of a reliable quantum computer. In this regard, topological quantum computing has been considered as an attractive solution for overcoming the related problems [1–4]. It processes quantum information in a nonlocal fashion, and in addition exploits the peculiarities of non-Abelian braiding statistics [5], allowing the performence of decoherence-free and fault-tolerant quantum logical operations [6]. In this context, so-called Majorana zero modes (MZMs) emerging at opposite ends of a one-dimensional (1D) spinless p-wave superconductor [7–10] exhibiting pronounced non-Abelian behavior associated topological degeneracy [5,11] have been proposed as elementary building blocks of a topological quantum computing hardware [12].

Although p-wave superconductivity is very rare in nature [13–16], it can be engineered in quasi-1D semiconducting nanowires with strong Rashba spin-orbit coupling, brought into close proximity with a conventional superconductor and placed in a strong external magnetic field parallel to the spin-orbit intrinsic field [8–10,17]. In this configuration, MZMs manifest themselves at the opposite ends of the topological superconducting segment [10,17]. They can be probed by means of tunneling spectroscopy experiments [18], where the appearance of a robust zero-bias anomaly (ZBP), verified in a set of experiments [19–24], was considered as direct evidence of their presence.

However, other physical mechanisms can be responsible for the formation of ZBPs, such as,e.g., Kondo effect [25,26] and formation of Andreev bound states (ABSs) [27–36]. These latter can be viewed as overlapping MZMs which can remain pinned at zero energy for a wide range of tunable parameters and even show perfect quantized conductance patterns [37,38], mimicking exactly the behavior expected for topologically protected MZMs. Strong disorder can also lead to such trivial ZBPs [37,39]. In order to distinguish between the ZBPs stemming from authentic topological MZMs and those arising from trivial zero-energy ABSs, a plethora of strategies have been proposed [30,40–47]. Among them, we draw attention to those which suggest experimental verification of "how topological" are the MZMs, either by means of the measurement of so-called topological quality factor [41] or degree of Majorana nonlocality [42,43].

In the present paper, we analyze the effect of the Coulomb interaction between electrons located in quantum dot (QD) and MZMs on the above-mentioned quantities. We study the low-energy spectrum of a hybrid system composed by a QD coupled to a topological superconducting section hosting MZMs at the opposite ends, as sketched in Fig. 1(a). Our findings reveal that the Coulomb interaction between the QD and the superconducting section leads to the additional overlap of the wave functions describing the individual MZMs, even when they are spatially far apart. Hence, the information about either the topological quality factor or degree of Majorana nonlocality cannot be unambiguously extracted in the interacting case. We discuss the effects of the Coulomb charging energy on topological operations, demonstrating that a braiding step must be performed diabatically with respect to the Coulomb strength in order to be considered as being topologically protected.

*Corresponding author: luciano.silianoricco@gmail.com

†Corresponding author: acfseridonio@gmail.com

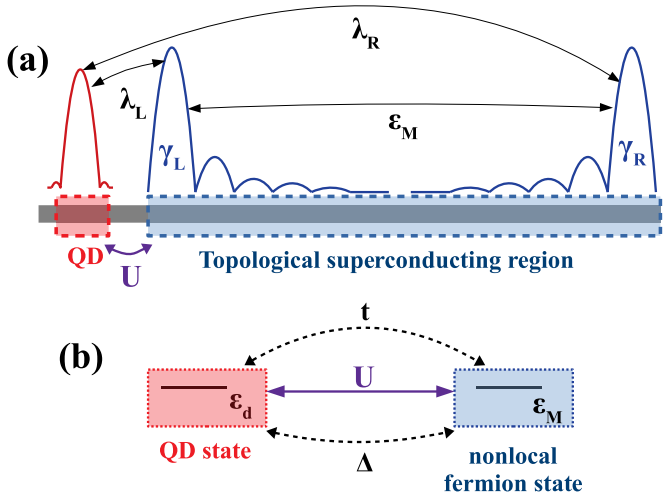

FIG. 1. (a) The sketch of the considered device, consisting of a hybrid topological superconducting nanowire in spinless regime (blue region), hosting left (γ_L) and right (γ_R) MZMs at the opposite ends, which are both coupled to a single level quantum dot (red region). λ_L and λ_R give the coupling amplitudes between the QD and left/right MZMs, respectively, while the parameter ε_M characterizes the spatial overlap between the wave functions describing the MZMs. There is also a Coulomb repulsion U between the QD and MZMs. (b) Equivalent scheme of the device. The topological superconducting section is now represented in terms of a nonlocal fermionic site with energy ε_M, constructed as a linear combination of spatially separated MZMs. In this formulation, U gives the strength of the intersite Coulomb charging repulsion between the QD and the nonlocal fermion. Moreover, the QD connects to the fermionic site via normal tunneling and crossed Andreev reflection terms, with amplitudes t and Δ, respectively.

II. MODEL AND METHODS

Consider a hybrid nanowire in the spinless regime [7] (i.e., when Zeeman splitting induced by strong external magnetic field parallel to the axis of the wire exceeds all other characteristic energies in the system), composed by a native quantum dot [22,43] with a single level coupled to both left and right MZMs located at the ends of the topological superconducting section of the corresponding nanowire [41,42,48–50] [see Fig. 1(a)]. The effective low-energy Hamiltonian describing such a system reads

$$\mathcal{H} = \varepsilon_d c_d^\dagger c_d + \imath\varepsilon_M \gamma_L\gamma_R + \lambda_L(c_d - c_d^\dagger)\gamma_L + \lambda_R(c_d + c_d^\dagger)\gamma_R + H_U, \quad (1)$$

where the operator $c_d^\dagger$ (c_d) creates (annihilates) an electron at the QD with energy ε_d and γ_L (γ_R) describes the left (right) Majorana mode emerging at the ends of the topological superconducting section. The Majorana operators satisfy self-conjugation $\gamma_i = \gamma_i^\dagger$, with $\{\gamma_i, \gamma_j\} = \delta_{i,j}(i = L, R)$ [10]. The amplitude of the spatial overlap between these MZMs is given by ε_M, which decays exponentially with the length L_{sc} of the superconducting nanowire segment [21,49,51]. The part of the Hamiltonian which describes the topological superconducting section hosting the MZMs hybridized with the QD is a well-established and widely used effective model derived from its corresponding tight-binding Hamiltonian and is independent of the Coulomb correlation [42]. It faithfully describes the low-energy spectrum of the entire system [41,42] by showing a good qualitative agreement with seminal experimental results [22,43].

In the continuum limit, the spatial wave function describing a MZM within the spinless condition reads [42]

$$\gamma_i = \frac{1}{\sqrt{2}}\int dx[\nu^{(i)}(x)c_x^\dagger + \nu^{(i)*}(x)c_x], \quad (2)$$

where $c_x^\dagger$ (c_x) creates (annihilates) electrons in the point x of the superconducting nanowire section, with the normalized wave functions $\nu^{(i)}(x)$ localized around the left ($i = L$) and right ($i = R$) MZMs. These opposite MZMs are related by the spatial inversion $\nu^{(R)}(x) = \imath\nu^{(L)}(L_{sc} - x)$ [42]. Within this description, the real coupling amplitudes between the QD and the left/right MZM read $\lambda_i \equiv \lambda a_0 \nu'^{(i)}(0)$, wherein $\nu'^{(i)}(0)$ is the leading term coming from the expansion of $\nu^{(i)}(x)$ around the first point of the superconducting section $x = 0$ [42,52] and a_0 is the tight-binding lattice parameter.

The last term in the Hamiltonian corresponds to the Coulomb repulsion between the electron of the QD, and MZMs. It can be easily constructed using the representation of a nonlocal fermion, which is a linear combination of two MZMs, $c_f^\dagger = (\gamma_L - \imath\gamma_R)/\sqrt{2}$, $n_f = c_f^\dagger c_f$. In this picture, the interaction can be simply read as $H_U = U n_d n_f$, where $n_d = c_d^\dagger c_d$ is an operator of the occupancy of the QD and [53]

$$U = \int d\vec{x}_d\vec{x}_f|\phi_d(\vec{x}_d)|^2\frac{e_0^2}{|\vec{x}_d - \vec{x}_f|}|\phi_f(\vec{x}_f)|^2, \quad (3)$$

where $\vec{x}_d$ and $\vec{x}_f$ are the positions of the QD and the fermionic site f, respectively, with the properly normalized wave functions $\phi_m(\vec{x}_m)$ $(m = d, f)$ and $e_0^2 = e^2/4\pi\varepsilon$, where e is the electronic charge at the QD (fermion state) and ε is the permittivity of the semiconducting region between the QD and the fermionic state f. Since the MZMs localized at the superconducting nanowire segment can be viewed as a fermionic state with nonlocal nature [Fig. 1(b)], Eq. (3) states that the Coulomb strength is inversely proportional to the distance $d \equiv |\vec{x}_d - \vec{x}_f|$ between the QD and the superconducting nanowire section. For hybrid experimental devices fabricated with InAs semiconducting nanowire partially covered by Al via epitaxial growth, the bare region of the parental semiconductor where the QD is formed has the length of ∼150 nm [22,43]. Considering typical values of permittivity for the InAs ($\varepsilon \sim 14.6\varepsilon_0$ [54,55]), one can estimate that $U \approx 0.10d^{-1}$ eV nm, yielding a Coulomb strength with magnitude between meV and μeV, depending on the size of the QD formed at the bare region nanowire.

Note that expressing the Majorana operators in terms of the fermionic ones, i.e., using the transformation $\gamma_L = (c_f^\dagger + c_f)/\sqrt{2}$ and $\gamma_R = \imath(c_f^\dagger - c_f)/\sqrt{2}$, the interaction term reads

$$H_U = U n_d n_f = U n_d\left(i\gamma_L\gamma_R + \tfrac{1}{2}\right). \quad (4)$$

It can be easily noted that the structure of this term closely resembles those for the second term in Eq. (1), $\imath\varepsilon_M\gamma_L\gamma_R$, which describes the overlap between the MZMs. Therefore, the QD-MZM repulsion leads to additional hybridization of the MZMs, whose amplitude Un_d depends on the QD occupancy. This has a dramatic effect on topological characteristics of the

system, as we will show below. A tight-binding description of H_U can be obtained by considering the MZMs structure in the continuum limit given by Eq. (2) into Eq. (4). Note that the intradot Coulomb interaction can be safely neglected, since only single occupancy is allowed in the QD within the spinless regime. Moreover, the Coulomb correlation between electrons in the superconducting section of the nanowire also can be safely neglected, since the attractive interaction between electrons forming the Cooper pairs is dominant over the Coulomb repulsion [53].

The system Hamiltonian [Eq. (1)] can be rewritten in terms of nonlocal fermionic operators $c_f^\dagger(c_f)$ as [10,50,56]

$$\mathcal{H} = \varepsilon_d c_d^\dagger c_d + \varepsilon_M c_f^\dagger c_f + (t c_d c_f^\dagger + \Delta c_d c_f + \text{H.c.}) + H_U + \text{const}, \tag{5}$$

where $\lambda_L = (t+\Delta)/\sqrt{2}$, $\lambda_R = \imath(\Delta - t)/\sqrt{2}$, and ε_M has now the meaning of a nonlocal fermionic excitation energy. The transport between the QD and topological wire is described in terms of a normal tunneling and crossed Andreev reflection with t and Δ being the corresponding amplitudes, which are both chosen real [41,50,56]. The MZMs are quadratically protected in the "sweet spot" $t = \Delta$ for $\varepsilon_M = U = 0$ [56], which corresponds to the ideal situation of well-isolated MZMs.

The system Hamiltonian given by Eq. (5) can be recast in the matrix form as

$$\mathcal{H} = \begin{pmatrix} 0 & 0 & 0 & -\Delta \\ 0 & \varepsilon_M & -t & 0 \\ 0 & -t & \varepsilon_d & 0 \\ -\Delta & 0 & 0 & \varepsilon_d + \varepsilon_M + U \end{pmatrix}, \tag{6}$$

where we have chosen the following basis $\{|00\rangle, |01\rangle, |10\rangle, |11\rangle\}$ for the number states $|n_d n_f\rangle$ [41,56]. It is worth noting that the results derived from Eq. (6) are invariant under change of sign of the parameters t and Δ. The same matrix Hamiltonian of Eq. (6) was previously adopted in Ref. [56] to describe a system of two QDs coupled via an s-wave superconductor in which the so-called "poor man's Majorana bound states" emerge. Distinct from our case, these states are not topologically protected and due to the charge screening induced by the superconductor set up between the QDs, the interdot Coulomb repulsion can be safely neglected.

The conductance through the system is determined by the density of states of the QD, which in the Lehmann representation reads [53]

$$\rho_d(V) = \frac{1}{\mathcal{Z}} \sum_{n,m} |\langle m|c_d^\dagger|n\rangle|^2 (e^{\beta E_n} + e^{\beta E_m}) \delta(V + E_n - E_m), \tag{7}$$

where $\beta = 1/k_B T$, $\mathcal{Z}$ is the partition function of Eq. (6) with a complete set of eigenstates $\{|(m)n\rangle\}$, and associated eigenvalues $E_{m(n)}$. For $T = 0$, the differential conductance through the QD $dI/dV \propto \rho_d(V)$ can be probed with a pair of metallic leads, with V being the corresponding bias voltage. Note that the attachment of metallic leads will broaden the peaks in the density of states, and the delta functions in Eq. (7) should be replaced by Lorentzians with broadening Γ [53,57]. For situations of finite temperature, the Lorentzians will be flattened, leading to a reduction of their heights. Thus, the condition $k_B T \ll \Gamma$ must be fulfilled in order to observe the corresponding peaks in the conductance profiles [23,58,59]. In our further analysis, however, we will be focusing on the position of the conductance peaks only and both the broadening and finite temperature effects will be neglected.

Equation (7) determines that a peak is registered in the conductance through the QD whenever a transition between the ground state of the system [Eq. (6)] and an excited state with opposite parity is allowed [41], i.e., when the matrix elements $|\langle m|c_d^\dagger|n\rangle| \neq 0$, and for $V = (E_m - E_n)$.

By taking into account the four possible eigenvalues of the QD-topological superconducting section extracted from Eq. (6) and considering the transition rules defined by Eq. (7), it is straightforward to show that a conductance peak will emerge at the low-energy spectrum of the system for $V = V_1 + V_2$, with

$$V_1 = \pm\tfrac{1}{2}[\sqrt{\epsilon_-^2 + (2t)^2} + \sqrt{(\epsilon_+ + U)^2 + (2\Delta)^2} - U] \tag{8}$$

and

$$V_2 = \pm\tfrac{1}{2}[\sqrt{\epsilon_-^2 + (2t)^2} - \sqrt{(\epsilon_+ + U)^2 + (2\Delta)^2} - U], \tag{9}$$

where V_1 describes the energy spectrum corresponding to the QD states (dashed green lines), while V_2 corresponds to the MZM spectrum (red lines), with $\epsilon_\pm = \varepsilon_d \pm \varepsilon_M$. For $U = 0$, we just recover the case described by Clarke [41], who also used the Lehmann representation for the noninteracting case.

Before presenting our results, it is worth discussing briefly the so-called topological quality factor, defined as

$$\mathcal{Q} = 1 - \frac{|\lambda_R|}{|\lambda_L|}, \tag{10}$$

proposed by Clarke [41] as a quantitative criterion allowing one to estimate if a system can be interpreted as topological for $\varepsilon_M \approx 0$. Well-separated MZMs correspond to the ideal topologically protected situation, wherein $\lambda_R = \varepsilon_M = 0$, yielding the highest quality factor $\mathcal{Q} = 1$. As the nonlocal nature of MZMs fades away, λ_R enhances, and $\mathcal{Q}$ approaches zero, the crossover to the topologically trivial case of overlapping MZMs, i.e., ABSs, occurs. The quality factor also can be viewed as an indirect way of estimating the charge of the MZMs, since for $\lambda_R \neq 0$ the opposite MZMs hybridize with each other via the QD, yielding a finite effective overlap $\varepsilon_M \neq 0$ between the MZMs. Although it can be smaller ($\lambda_R \gg \varepsilon_M$), this effective overlap via QD plays the role of a discrete energy level in the fermionic basis [Eq. (5)], which can be empty or fulfilled according to its relative position to the Fermi level introduced by the presence of leads in an experimental device, thus estimating the amount of charge in the fermionic state made by the MZMs. $\mathcal{Q}$ is directly related with the so-called degree of Majorana nonlocality introduced by Prada *et al.* [42] and experimentally studied by Deng *et al.* [43].

III. RESULTS AND DISCUSSION

In the following analysis, we adopt the QD-left MZM coupling amplitude λ_L as the energy unit. For practical situations whose QD is coupled to metallic leads λ_L scales with the QD level broadening Γ [57], which typically has the order

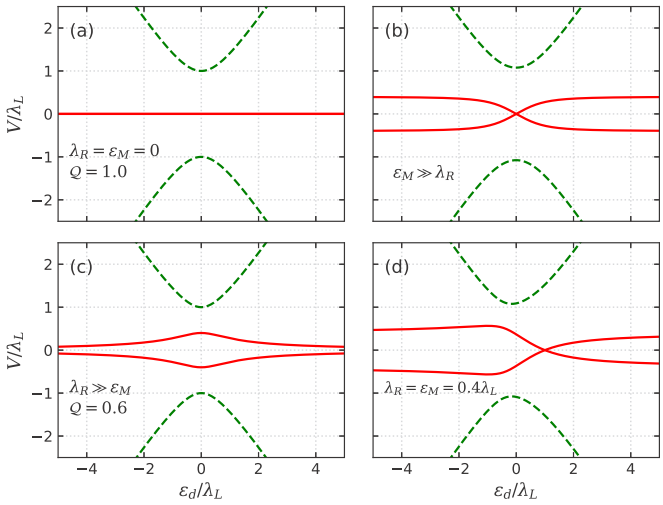

FIG. 2. Low-energy spectrum characterizing the conductance profiles [Eqs. (8) and (9)] as a function of the QD energy-level ε_d and applied bias-voltage V for non interacting case ($U = 0$). The red lines describe the position of the peak, related to the states of the topological superconducting section hosting MZMs, dashed-green lines correspond to the QD states. (a) The case of well-separated MZMs ($\lambda_R = \varepsilon_M = 0$), yielding the highest topological quality factor, $\mathcal{Q} = 1$. Horizontal red line corresponds to the robust ZBP. (b) The case, when the wavefunctions describing the MZMs at the opposite ends of the topological section are strongly overlapping ($\varepsilon_M \gg \lambda_R$). ZBP is splitted, producing characteristic bowtie, or double-fork, pattern. (c) The case of a finite overlap between the QD and the right MZM, with $\mathcal{Q} = 0.6$, $\varepsilon_M = 0$. (d) The case, when the overlap between the MZMs is comparable with those between the QD and the right MZM.

of a few μeV for QD experimental setups [48,58]. In this scenario, the condition $\lambda_L > \Gamma$ must be fulfilled for ensuring that any features of the QD-MZMs low-energy spectrum are not spoiled by the QD-leads hybridization [58].

A. Noninteracting case

We start from a brief discussion of the results for the noninteracting case ($U = 0$) previously obtained by Clarke [41], just in order to better understand the interacting case. We emphasize that the main focus of the present work is to study the effects of the aforementioned Coulomb intersite correlation U, not proposing a measurement protocol as in Ref. [41].

In Fig. 2, the corresponding low-energy spectrum is presented. The ideal situation of well-separated MZMs is shown in Fig. 2(a). There is no overlap between either the wave function of the QD and that describing the right MZM ($\lambda_R = 0$), or between the wave functions describing the right and left MZMs ($\varepsilon_M = 0$), and $\mathcal{Q} = 1$. This corresponds to the perfect topological case with quadratically protected MZMs [56], for which there is a robust single zero-bias conductance peak which remains pinned to zero when the QD energy level is tuned (red horizontal line).

The situation drastically changes when a finite overlap between the MZMs is taken into account ($\varepsilon_M \neq 0$), as shown in Fig. 2(b). In this case, the spectrum corresponding to the MZMs (red lines) splits, revealing the crossing at $\varepsilon_d = 0$, the pattern known as *bowtie* [42] or *double-fork* profile [50].

Figure 2(c) illustrates the case when the overlap amplitude λ_R between the QD and the right MZM is finite and $\varepsilon_M \approx 0$, and the corresponding topological quality factor is $\mathcal{Q} = 0.6$. The fact that $\mathcal{Q} < 1$ introduces a constraint for topological quantum operations, as we shall see later. These quasi-MZMs are characterized by a *diamondlike* profile [42,43] for the split ZBP.

Finally, in Fig. 2(d) we illustrate the case where $\lambda_R = \varepsilon_M$ and a highly asymmetric bowtie is revealed. Both Figs. 2(c) and 2(d) correspond quite well to the experimental conductance profiles reported by Deng. *et al.* [22], which means that the experimental prototype was in fact in the trivial phase [41,42].

B. Interacting case

The low-energy spectrum of the system drastically changes when the Coulomb interaction U between the QD and the topological superconducting section hosting MZMs is taken into account. For typical experiments with hybrid devices composed by a QD and a topological superconducting nanowire, the intradot Coulomb interaction has the magnitude of a few meV [22,42,43] in the Coulomb blockade regime. However, in the present case of spinless regime, only the interdot Coulomb interaction becomes relevant and has the order of μeV for double quantum dot experimental arrangements hybridized with leads [60,61], which is within our previous estimate provided by Eq. (3). Since we are not interested in studying the effects related to the strong capacitive coupling limit characterized by $U \gg \lambda_L$ [62–64], we consider U and λ_L magnitudes on an equal footing.

As was already mentioned, in the representation of nonlocal fermions this interaction describes a simple charge repulsion, while in the basis of MZMs it has a structure similar to those terms describing the overlap between the MZMs [see Eq. (4)]. This leads to the splitting of the ZBP and the formation of a bowtie structure even for the seemingly ideal case, corresponding to $\lambda_R = \varepsilon_M = 0$, as shown in Fig. 3(a). In the fermionic representation [Eq. (5)], this ideal case corresponds to a QD coupled to a highly nonlocal fermion with zero energy $\varepsilon_M = 0$ and finite Coulomb correlation between them. In a real experimental apparatus with the presence of metallic leads hybridized to the QD and the corresponding broadening Γ, the case of $\varepsilon_M = 0$ but $U \neq 0$ can be achieved in the so-called intermediate valence regime [65] in which the charge fluctuations are allowed in the localized states. This regime takes place when the state ε_M approaches the Fermi level ε_F of the leads, so that $\varepsilon_M - \varepsilon_F \sim \Gamma$ or $\varepsilon_M + U - \varepsilon_F \sim \Gamma$. The unexpected loss of robustness of the ZBP shown in Fig. 3(a) is precisely owing to the Coulomb correlation, which effectively overlaps the wave functions of the MZMs having the QD as an intermediate, in accordance with Eq. (4). Note that as in the considered case the amplitude of the overlap depends on the occupancy of the dot, the corresponding bowtie structure becomes slightly distorted, forming a crooked double fork with the crossing point slightly shifted from $\varepsilon_d = 0$. The information about the strength of the Coulomb interaction can be extracted from such a

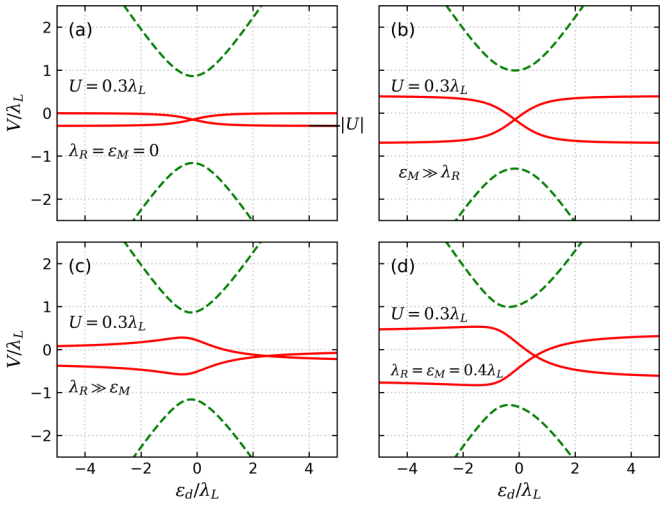

FIG. 3. Low-energy spectrum characterizing the conductance profiles [Eqs. (8) and (9)] as a function of the QD energy level ε_d and applied bias voltage V for the interacting case ($U \neq 0$). The red lines describe the position of the peak, related to the states of the topological superconducting section hosting MZMs; dashed-green lines correspond to the QD states. (a) The case of well-separated MZMs ($\lambda_R = \varepsilon_M = 0$), yielding the highest topological quality factor, $\mathcal{Q} = 1$. The robust ZBA, represented by the horizontal red line in Fig. 2(a) is destroyed by the intersite repulsion, and transforms into bowtie profile. (b) The case when the wave functions describing the MZMs at the opposite ends of the topological section are strongly overlapping ($\varepsilon_M \gg \lambda_R$). The finite U leads tothe appearance of slight asymmetry in the bowtie profile, and greater splitting of the lines. (c) The case of a finite overlap between the QD and the right MZM, $\lambda_R \neq 0$, $\varepsilon_M = 0$. The symmetric diamond profile, characteristic to the noninteracting case, transforms into asymmetric bowtie due to interaction induced hybridization of MZMs. (d) The case when the overlap between the MZMs is comparable with those between the QD and the right MZM. Interactions do not qualitatively change the figures, increasing the degree of asymmetry and splitting.

low-energy spectrum profile, as indicated in the corresponding Fig. 3(a).

If the overlap between the MZMs is already present ($\varepsilon_M \neq 0$), Coulomb correlations contribute to the additional vertical distancing of the bowtie lines, together with a horizontal shift of the crossing point from $\varepsilon_d = 0$, as shown in Fig. 3(b).

Figure 3(c) illustrates the regime for which the concept of the quality factor was originally introduced, namely, $\lambda_R \gg \varepsilon_M$. One can clearly see that the account of the Coulomb corrections destroys the symmetric *diamond* shape characteristic to the noninteracting case and leads to the appearance of the crossing and formation of an asymmetric bowtie profile, which is a direct consequence of the interaction induced hybridization of MZMs. As for the case when λ_R and ε_M are comparable, the situation is qualitatively similar for the noninteracting and interacting cases, the quantitative difference being that the asymmetry of the profiles and the splitting between the lines is enhanced in the interacting regime [see Fig. 3(d)].

Using Eqs. (8) and (9), one can obtain the expression for the position of the crossing of the red lines in

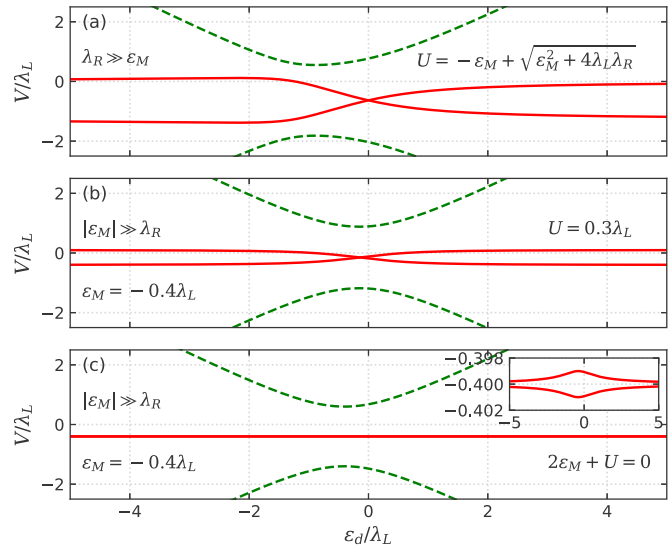

FIG. 4. Low-energy spectrum characterizing the conductance profiles [Eqs. (8) and (9)] as a function of the QD energy level ε_d and applied bias voltage V for the interacting case ($U \neq 0$). The red lines describe the position of the peak, related to the states of the topological superconducting section hosting MZMs; dashed-green lines correspond to the QD states. (a) The case wherein the value of U corresponds to $\varepsilon_{\text{cross}} = 0$ [Eq. (11)] for ε_M and $\lambda_R \neq 0$, showing a symmetric profile in relation to $\varepsilon_d = 0$. (b) The overlap strength between the MZMs is negative, but holds the condition $|\varepsilon_M| \gg \lambda_R$. (c) Same situation of the panel above, but for the condition $2\varepsilon_M + U = 0$, yielding an indistinguishable splitting of the states describing the MZMs. The zoomed spectrum near $V = 0$ is shown in the inset panel.

Figs. 2 and 3:

$$\varepsilon_{\text{cross}} = \frac{2\lambda_L\lambda_R}{(2\varepsilon_M + U)} - \frac{U}{2}. \tag{11}$$

For $\varepsilon_M \to 0$, $U \to 0$, and $\lambda_L \neq 0$, $\varepsilon_{\text{cross}} \to \infty$ and then, there is no crossing between the near-zero-energy states, as indeed one can verify in Fig. 2(c). However, for the interacting case wherein $U = 0.3\lambda_L$, $\lambda_R = 0.4\lambda_L$, and $\varepsilon_M \approx 0$, we obtain $\varepsilon_{\text{cross}} \approx 2.5\lambda_L$, which corresponds to Fig. 3(c).

Equation (11), one can verify that $U = -\varepsilon_M + \sqrt{\varepsilon_M^2 + 4\lambda_L\lambda_R}$ gives the physical solution for $\varepsilon_{\text{cross}} = 0$, with ε_M and $\lambda_L \neq 0$, as shown in Fig. 4(a). By fulfilling this condition, the asymmetric profile of the near-zero-energy states in relation to $\varepsilon_d = 0$ [Fig. 3(c)] is symmetrized.

Figure 4(b) depicts the case of $\varepsilon_M < 0$ and $|\varepsilon_M| \gg \lambda_R$. In the Majorana basis [Eq. (1)], this situation corresponds to a negative overlap strength between the MZMs, once ε_M is proportional to a cosine function, showing an oscillatory behavior for shorter nanowires [49]. A comparison between Figs. 3(b) and 4(b) shows that the negative value of ε_M reduces the width of the near-zero-energy splitting in the interacting picture. This feature points out that the splitting strength of the states which correspond to the MZMs (red lines) is proportional to $\varepsilon_M + U$. If one considers, e.g., the condition $2\varepsilon_M + U = 0$ with $\varepsilon_M < 0$ [Fig. 4(c)], the splitting is indistinguishable (see the zoomed inset panel), yielding an apparent plateau shifted from $V = 0$.

C. Effects of the interaction on topological operations

Both the quality factor $\mathcal{Q} < 1$ ($\lambda_R \neq 0$) and spatial overlap $\varepsilon_M \neq 0$ between the MZMs introduce some restrictions for performing topological operations given by braiding processes [1,6,41,66,67]. Specifically, an exchange operation involving MZMs (braid step) must be performed very quickly with respect to characteristic times defined by the coupling λ_R and the overlap ε_M, so that the system responds as if it were topologically protected ($\lambda_R = \varepsilon_M = 0$, $\mathcal{Q} = 1$). Once Coulomb correlations in the considered system induce the additional overlap of the MZMs [see Eq. (4)], it is natural to infer that a braiding operation also must be performed diabatically in relation to U. All these constraints imply that [41]

$$\frac{\hbar}{\lambda_L \tau_{\rm op}}, \quad \frac{\hbar}{\varepsilon_M \tau_{\rm op}}, \quad \frac{\hbar}{U \tau_{\rm op}} \ll 1, \tag{12}$$

where $\tau_{\rm op}$ is the operational time to take a braid step.

IV. CONCLUSIONS

We have studied the low-energy spectrum of a hybrid system consisting of a topological nanowire hosting a pair of MZMs at its opposite ends, and a QD simultaneously coupled to both them. It was demonstrated that the Coulomb interaction between the dot and the superconducting section leads to an additional hybridization of the MZMs, which strongly affects the density of states of the system and modifies the corresponding conductance profiles. It is shown that the interactions compromise the analysis of the topological quality factor, introduced as a quantitative measure of the level of the degree of topological protection in a noninteracting system. This leads to the additional constraint for the braiding operation in the quantum computing process, which should be performed diabatically with respect to the Coulomb charging energy.

ACKNOWLEDGMENTS

L.S.R. acknowledges support from São Paulo Research Foundation (FAPESP), Grant No. 2015/23539-8. J.E.S. acknowledges support from the Coordenao de Aperfeiçoamento de Pessoal de Nível Superior–Brasil (CAPES)–Finance Code 001 (Ph.D. fellowship). Y.M. and I.A.S. acknowledge support from the Ministry of Science and Higher Education of Russian Federation, Goszadanie No. 2019-1246 and ITMO 5-100 Program. A.C.S. acknowledges support from Brazilian National Council for Scientific and Technological Development (CNPq), Grant No. 305668/2018-8.

[1] J. Alicea, Y. Oreg, G. Refael, F. von Oppen, and M. P. A. Fisher, Non-Abelian statistics and topological quantum information processing in 1D wire networks, Nat. Phys. **7**, 412 (2011).

[2] A. Kitaev, Fault-tolerant quantum computation by anyons, Ann. Phys. **303**, 2 (2003).

[3] M. H. Freedman, A. Kitaev, M. J. Larsen, and Z. Wang, Topological quantum computation, Bull. Am. Math. Soc. **40**, 31 (2003).

[4] C. Knapp, M. Zaletel, D. E. Liu, M. Cheng, P. Bonderson, and C. Nayak, The Nature and Correction of Diabatic Errors in Anyon Braiding, Phys. Rev. X **6**, 041003 (2016).

[5] C. Nayak, S. H. Simon, A. Stern, M. Freedman, and S. Das Sarma, Non-Abelian anyons and topological quantum computation, Rev. Mod. Phys. **80**, 1083 (2008).

[6] D. Aasen, M. Hell, R. V. Mishmash, A. Higginbotham, J. Danon, M. Leijnse, T. S. Jespersen, J. A. Folk, C. M. Marcus, K. Flensberg, and J. Alicea, Milestones Toward Majorana-Based Quantum Computing, Phys. Rev. X **6**, 031016 (2016).

[7] A. Y. Kitaev, Unpaired Majorana fermions in quantum wires, Phys. Usp. **44**, 131 (2001).

[8] J. Alicea, New directions in the pursuit of Majorana fermions in solid state systems, Rep. Prog. Phys. **75**, 076501 (2012).

[9] S. R. Elliott and M. Franz, Colloquium: Majorana fermions in nuclear, particle, and solid-state physics, Rev. Mod. Phys. **87**, 137 (2015).

[10] R. Aguado, Majorana quasiparticles in condensed matter, Riv. Nuovo Cimento **40**, 523 (2017).

[11] D. J. Clarke, J. D. Sau, and S. Das Sarma, Probability and braiding statistics in Majorana nanowires, Phys. Rev. B **95**, 155451 (2017).

[12] S. Plugge, A. Rasmussen, R. Egger, and K. Flensberg, Majorana box qubits, New J. Phys. **19**, 012001 (2017).

[13] A. P. Mackenzie and Y. Maeno, The superconductivity of Sr_2RuO_4 and the physics of spin-triplet pairing, Rev. Mod. Phys. **75**, 657 (2003).

[14] G. Moore and N. Read, Nonabelions in the fractional quantum Hall effect, Nucl. Phys. B **360**, 362 (1991).

[15] N. B. Kopnin and M. M. Salomaa, Mutual friction in superfluid ^{3}He: Effects of bound states in the vortex core, Phys. Rev. B **44**, 9667 (1991).

[16] G. E. Volovik, Fermion zero modes on vortices in chiral superconductors, JETP Lett. **70**, 609 (1999).

[17] R. M. Lutchyn, J. D. Sau, and S. Das Sarma, Majorana Fermions and a Topological Phase Transition in Semiconductor-Superconductor Heterostructures, Phys. Rev. Lett. **105**, 077001 (2010).

[18] R. M. Lutchyn, E. P. A. M. Bakkers, L. P. Kouwenhoven, P. Krogstrup, C. M. Marcus, and Y. Oreg, Majorana zero modes in superconductor-semiconductor heterostructures, Nat. Rev. Mater. **3**, 52 (2018).

[19] V. Mourik, K. Zuo, S. M. Frolov, S. R. Plissard, E. P. A. M. Bakkers, and L. P. Kouwenhoven, Signatures of Majorana fermions in hybrid superconductor-semiconductor nanowire devices, Science **336**, 1003 (2012).

[20] P. Krogstrup, N. L. B. Ziino, W. Chang, S. M. Albrecht, M. H. Madsen, E. Johnson, J. Nygård, C. M. Marcus, and T. S. Jespersen, Epitaxy of semiconductor-superconductor nanowires, Nat. Mater. **14**, 400 (2015).

[21] S. M. Albrecht, A. Higginbotham, M. Madsen, F. Kuemmeth, T. S. Jespersen, J. Nygård, P. Krogstrup, and C. Marcus, Exponential protection of zero modes in Majorana islands, Nature (London) **531**, 206 (2016).

[22] M. T. Deng, S. Vaitiekenas, E. B. Hansen, J. Danon, M. Leijnse, K. Flensberg, J. Nygård, P. Krogstrup, and C. M. Marcus,

Majorana bound state in a coupled quantum-dot hybrid-nanowire system, Science **354**, 1557 (2016).

[23] F. Nichele, A. C. C. Drachmann, A. M. Whiticar, E. C. T. O'Farrell, H. J. Suominen, A. Fornieri, T. Wang, G. C. Gardner, C. Thomas, A. T. Hatke, P. Krogstrup, M. J. Manfra, K. Flensberg, and C. M. Marcus, Scaling of Majorana Zero-Bias Conductance Peaks, Phys. Rev. Lett. **119**, 136803 (2017).

[24] Ö. Gül, H. Zhang, J. D. S. Bommer, M. W. A. de Moor, D. Car, S. R. Plissard, E. P. A. M. Bakkers, A. Geresdi, K. Watanabe, T. Taniguchi, and L. P. Kouwenhoven, Ballistic Majorana nanowire devices, Nat. Nanotechnol. **13**, 192 (2018).

[25] S. M. Cronenwett, T. H. Oosterkamp, and L. P. Kouwenhoven, A tunable Kondo effect in quantum dots, Science **281**, 540 (1998).

[26] D. Goldhaber-Gordon, H. Shtrikman, D. Mahalu, D. Abusch-Magder, U. Meirav, and M. A. Kastner, Kondo effect in a single-electron transistor, Nature (London) **391**, 156 (1998).

[27] G. Kells, D. Meidan, and P. W. Brouwer, Near-zero-energy end states in topologically trivial spin-orbit coupled superconducting nanowires with a smooth confinement, Phys. Rev. B **86**, 100503(R) (2012).

[28] E. J. H. Lee, X. Jiang, M. Houzet, R. Aguado, C. M. Lieber, and S. De Franceschi, Spin-resolved Andreev levels and parity crossings in hybrid superconductor-semiconductor nanostructures, Nat. Nanotechnol. **9**, 79 (2013).

[29] C.-X. Liu, J. D. Sau, T. D. Stanescu, and S. Das Sarma, Andreev bound states versus Majorana bound states in quantum dot-nanowire-superconductor hybrid structures: Trivial versus topological zero-bias conductance peaks, Phys. Rev. B **96**, 075161 (2017).

[30] C.-X. Liu, J. D. Sau, and S. Das Sarma, Distinguishing topological Majorana bound states from trivial Andreev bound states: Proposed tests through differential tunneling conductance spectroscopy, Phys. Rev. B **97**, 214502 (2018).

[31] M. Hell, K. Flensberg, and M. Leijnse, Distinguishing Majorana bound states from localized Andreev bound states by interferometry, Phys. Rev. B **97**, 161401(R) (2018).

[32] Y.-H. Lai, J. D. Sau, and S. Das Sarma, Presence versus absence of end-to-end nonlocal conductance correlations in Majorana nanowires: Majorana bound states versus Andreev bound states, Phys. Rev. B **100**, 045302 (2019).

[33] J. Chen, B. D. Woods, P. Yu, M. Hocevar, D. Car, S. R. Plissard, E. P. A. M. Bakkers, T. D. Stanescu, and S. M. Frolov, Ubiquitous Non-Majorana Zero-Bias Conductance Peaks in Nanowire Devices, Phys. Rev. Lett. **123**, 107703 (2019).

[34] P. Marra and M. Nitta, Topologically nontrivial Andreev bound states, Phys. Rev. B **100**, 220502(R) (2019).

[35] T. D. Stanescu and S. Tewari, Robust low-energy Andreev bound states in semiconductor-superconductor structures: Importance of partial separation of component Majorana bound states, Phys. Rev. B **100**, 155429 (2019).

[36] A. Vuik, B. Nijholt, A. R. Akhmerov, and M. Wimmer, Reproducing topological properties with quasi-Majorana states, SciPost Phys. **7**, 61 (2019).

[37] H. Pan and S. Das Sarma, Physical mechanisms for zero-bias conductance peaks in Majorana nanowires, Phys. Rev. Res. **2**, 013377 (2020).

[38] H. Pan, W. S. Cole, J. D. Sau, and S. Das Sarma, Generic quantized zero-bias conductance peaks in superconductor-semiconductor hybrid structures, Phys. Rev. B **101**, 024506 (2020).

[39] D. Bagrets and A. Altland, Class *d* Spectral Peak in Majorana Quantum Wires, Phys. Rev. Lett. **109**, 227005 (2012).

[40] A. Schuray, L. Weithofer, and P. Recher, Fano resonances in Majorana bound states–quantum dot hybrid systems, Phys. Rev. B **96**, 085417 (2017).

[41] D. J. Clarke, Experimentally accessible topological quality factor for wires with zero energy modes, Phys. Rev. B **96**, 201109(R) (2017).

[42] E. Prada, R. Aguado, and P. San-Jose, Measuring Majorana nonlocality and spin structure with a quantum dot, Phys. Rev. B **96**, 085418 (2017).

[43] M.-T. Deng, S. Vaitiekėnas, E. Prada, P. San-Jose, J. Nygård, P. Krogstrup, R. Aguado, and C. M. Marcus, Nonlocality of Majorana modes in hybrid nanowires, Phys. Rev. B **98**, 085125 (2018).

[44] C. Moore, C. Zeng, T. D. Stanescu, and S. Tewari, Quantized zero-bias conductance plateau in semiconductor-superconductor heterostructures without topological Majorana zero modes, Phys. Rev. B **98**, 155314 (2018).

[45] J. E. Sanches, L. S. Ricco, W. N. Mizobata, Y. Marques, M. de Souza, I. A. Shelykh, and A. C. Seridonio, Majorana molecules and their spectral fingerprints, Phys. Rev. B **102**, 075128 (2020).

[46] L. S. Ricco, J. E. Sanches, Y. Marques, M. de Souza, M. S. Figueira, I. A. Shelykh, and A. C. Seridonio, Topological isoconductance signatures in Majorana nanowires, arXiv:2004.14182.

[47] P. Yu, J. Chen, M. Gomanko, G. Badawy, E. P. A. M. Bakkers, K. Zuo, V. Mourik, and S. M. Frolov, Non-Majorana states yield nearly quantized conductance in superconductor-semiconductor nanowire devices, arXiv:2004.08583.

[48] E. Vernek, P. H. Penteado, A. C. Seridonio, and J. C. Egues, Subtle leakage of a Majorana mode into a quantum dot, Phys. Rev. B **89**, 165314 (2014).

[49] L. S. Ricco, V. L. Campo, I. A. Shelykh, and A. C. Seridonio, Majorana oscillations modulated by Fano interference and degree of nonlocality in a topological superconducting-nanowire–quantum-dot system, Phys. Rev. B **98**, 075142 (2018).

[50] L. S. Ricco, F. A. Dessotti, I. A. Shelykh, M. S. Figueira, and A. C. Seridonio, Tuning of heat and charge transport by Majorana fermions, Sci. Rep. **8**, 2790 (2018).

[51] J. Klinovaja and D. Loss, Composite Majorana fermion wave functions in nanowires, Phys. Rev. B **86**, 085408 (2012).

[52] E. Prada and F. Sols, Entangled electron current through finite size normal-superconductor tunneling structures, Eur. Phys. J. B **40**, 379 (2004).

[53] H. Bruus and K. Flensberg, *Many-Body Quantum Theory in Condensed Matter Physics: An Introduction*, Oxford Graduate Texts (Oxford University Press, New York, 2004).

[54] S. Adachi, J. Appl. Phys. **53**, 8775 (1982).

[55] K. Brennan and K. Hess, High field transport in GaAs, InP and InAs, Solid-State Electron. **27**, 347 (1984).

[56] M. Leijnse and K. Flensberg, Parity qubits and poor man's Majorana bound states in double quantum dots, Phys. Rev. B **86**, 134528 (2012).

[57] P. W. Anderson, Localized magnetic states in metals, Phys. Rev. **124**, 41 (1961).

[58] D. A. Ruiz-Tijerina, E. Vernek, L. G. G. V. Dias da Silva, and J. C. Egues, Interaction effects on a Majorana zero mode leaking into a quantum dot, Phys. Rev. B **91**, 115435 (2015).

[59] D. Rainis, L. Trifunovic, J. Klinovaja, and D. Loss, Towards a realistic transport modeling in a superconducting nanowire with Majorana fermions, Phys. Rev. B **87**, 024515 (2013).

[60] D. T. McClure, L. DiCarlo, Y. Zhang, H.-A. Engel, C. M. Marcus, M. P. Hanson, and A. C. Gossard, Tunable Noise Cross Correlations in a Double Quantum Dot, Phys. Rev. Lett. **98**, 056801 (2007).

[61] A. Hübel, K. Held, J. Weis, and K. v. Klitzing, Correlated Electron Tunneling through Two Separate Quantum Dot Systems with Strong Capacitive Interdot Coupling, Phys. Rev. Lett. **101**, 186804 (2008).

[62] I. H. Chan, R. M. Westervelt, K. D. Maranowski, and A. C. Gossard, Strongly capacitively coupled quantum dots, Appl. Phys. Lett. **80**, 1818 (2002).

[63] Y. Okazaki, S. Sasaki, and K. Muraki, Spin-orbital Kondo effect in a parallel double quantum dot, Phys. Rev. B **84**, 161305(R) (2011).

[64] F.-L. Sun, Y.-D. Wang, J.-H. Wei, and Y.-J. Yan, Capacitive coupling induced Kondo Fano interference in side-coupled double quantum dots, Chin. Phys. B **29**, 067204 (2020).

[65] A. C. Hewson, *The Kondo Problem to Heavy Fermions*, Cambridge Studies in Magnetism (Cambridge University Press, Cambridge, UK, 1993).

[66] J. D. Sau, D. J. Clarke, and S. Tewari, Controlling non-Abelian statistics of Majorana fermions in semiconductor nanowires, Phys. Rev. B **84**, 094505 (2011).

[67] B. I. Halperin, Y. Oreg, A. Stern, G. Refael, J. Alicea, and F. von Oppen, Adiabatic manipulations of Majorana fermions in a three-dimensional network of quantum wires, Phys. Rev. B **85**, 144501 (2012).